Model Validations for Low-GWP refrigerants in Mini-Split Air Conditioning Units

ABSTRACT

To identify low GWP (global warming potential) refrigerants to replace R-22 and R-410A, extensive experimental evaluations were conducted for multiple candidates of refrigerant at the standard test conditions and at high-ambient conditions with outdoor temperature varying from 27.8°C to 55.0°C. In the study, R-22 was compared to propane (R-290), DR-3, ARM-20B, N-20B and R-444B in a mini-split air conditioning unit originally designed for R-22; R-410A was compared to R-32, DR-55, ARM-71A, L41-2 (R-447A) in a mini-split unit designed for R-410A. To reveal physics behind the measured performance results, thermodynamic properties of the alternative refrigerants were analysed. In addition, the experimental data was used to calibrate a physics-based equipment model, i.e. ORNL Heat Pump Design Model (HPDM). The calibrated model translated the experimental results to key calculated parameters, i.e. compressor efficiencies, refrigerant side two-phase heat transfer coefficients, corresponding to each refrigerant. These calculated values provide scientific insights on the performance of the alternative refrigerants and are useful for other applications beyond mini-split air conditioning units.

Key Words: Low-GWP Refrigerant, Mini-Split Air Conditioning Unit, Model, High Ambient Condition.

Introduction

The use of hydrofluorocarbon (HFC) refrigerants as non-ozone-depleting fluids alternatives for air-conditioning and refrigeration equipment was adopted by the developed countries during the ozone-depleting substances (ODS) phase-out as described in the Montreal Protocol (Ozone Secreteriat, 2016). Unfortunately, the commonly used HFCs have higher global warming potential (GWP) compared to the refrigerants that they replaced, for example, R-410A has a GWP 1924, and R-22 has a GWP 1760, which are thousands of times higher than natural refrigerants like CO_2.

HFCs currently account for only 1% of greenhouse gas emissions, but their use is growing rapidly, by as much as 10 to 15% per year, primarily because of their use as replacements for ODS and the increasing use of air conditioners globally, as reported by Ramanathan and Xu (2010 and 2013). Furthermore, according to the Montreal Protocol, Developing Countries, Article 5 Countries, have started their phase-down schedule for ODS. As such, finding suitable lower GWP refrigerants for HFC and hydrochlorofluorocarbon (HCFC) refrigerants is timely and will avoid a costly two-step transition from HCFC to HFC and then from HFC to lower-GWP refrigerants. Therefore, there is potential for significant reduction in greenhouse gas emissions through the substitution of high-GWP HFCs and HCFCs with lower-GWP alternatives.

While progress toward widespread application of low-GWP refrigerants continues, only limited information regarding the performance of the most commonly proposed low-GWP refrigerants is available. Abdelaziz and Shrestha (2016) conducted extensive experimental tests to assess low GWP alternative refrigerants as drop-in replacements in two mini-split air conditioning units designed for high-ambient conditions. One unit was designed for R-22 and the other for R-410A. Table 1 shows the R-22 alternatives; Table 2 shows the R-410A alternatives evaluated by Abdelaziz and Shrestha (2016). In these tables, the temperature glides in the condenser were calculated as the difference between the saturated vapour temperature and liquid temperature at the pressure corresponding to 115°F (46.1°C) dew point; and glides in the evaporator was calculated at the pressure corresponding to 50°F (18°C) dew point.

Table 1. Alterative Low GWP Replacements for R-22

Refrigerant	GWP AR4	GWP AR5	Safety Class	Glide in Condenser [K]	Glide in Evaporator [K]	Critical Temperature [C]
R-22	1810	1760	A1	0.0	0.0	96.16
Propane (R-290)	3	3	A3	0.0	0.0	96.74
DR-3[a]	148	146	A2L	6.5	7.7	88.47
ARM-20B[b]	251	251	A2L	5.3	6.0	88.74
N-20B[c]	988	904	A1	4.6	5.4	89.62
R-444B[d]	295	295	A2L	7.6	8.9	92.11

[a.] DR-3 has mass-based compositions of R-32 (0.215)/R-1234yf (0.785).

[b.] ARM-20B has mass-based compositions of R-32 (0.35)/R-1234yf (0.55)/R-152a (0.1).

[c] N-20B has mass-based compositions of R-32 (0.13)/R-125 (0.13)/R-134a (0.31)/R-1234yf (0.43).

[d] R-444B has mass-based compositions of R-32 (0.415)/ R-1234ze(E) (0.485)/R-152a (0.1).

Table 2. Alterative Low GWP Replacements for R-410A

Refrigerant	GWP AR4	GWP AR5	Safety Class	Glide in Condenser [K]	Glide in Evaporator [K]	Critical Temperature [C]
R-410A[a]	2088	1924	A1	0.1	0.1	71.34
R-32	675	677	A2L	0.0	0.0	78.12
DR-55[b]	698	676	A2L	1.2	1.3	79.68
ARM-71A[c]	460	461	A2L	1.8	2.1	81.52
L41-2 (R-447A)[d]	583	572	A2L	3.8	4.6	82.63

[a] R-410A has mass-based compositions of R-32 (0.5)/R-125 (0.5).

[b] DR-55 has mass-based compositions of R-32 (0.67)/R-125 (0.07)/R-1234yf (0.26).

[c] ARM-71A has mass-based compositions of R-32 (0.68)/R-1234yf (0.26)/ R-1234ze(E) (0.06).

[d] L41-2 has mass-based compositions of R-32 (0.68)/R-125 (0.035)/R-1234ze(E) (0.285).

The test conditions from Abdelaziz and Shrestha (2016) are listed in Table 3. They reported the measured air side capacities and Energy Efficiency Ratios, and compared performances of different refrigerants. Table 4 compares the R-22 alternatives, while Table 5 compares the R-410A alternatives. The experimental results were obtained via a soft-optimized process, as follows,

1. Select capillary tube length using appropriate correlations (ASHRAE, 2002, and the method used by S. Yana Motta, 1999) and fabricate.
2. Run charge optimization procedure at the AHRI A condition to maximize COP and decide the optimized charge of $M_{opt,ref\#}$: collect steadystate data for 10 minutes at each condition.
3. Run the unit with $M_{opt,ref\#}$ and the selected capillary tube at T3 conditions to ensure adequate subcooling and superheating; if not, adjust the charge accordingly (approximately 2 oz. at a time with 10 min of steady-state data collected).
4. Evaluate the system performance for all test conditions listed in Table 3.

Table 3. Test Conditions

Test condition	Outdoor [a]	Indoor			
	Dry-bulb temperature	Dry-bulb temperature	Wet-bulb temperature	Dew point temperature [b]	Relative humidity [b]
AHRI B [c]	27.8 (82)	26.7 (80.0)	19.4 (67)	15.8 (60.4)	50.9
AHRI A [c]	35.0 (95)	26.7 (80.0)	19.4 (67)	15.8 (60.4)	50.9
T3* [d]	46 (114.8)	26.7 (80.0)	19 (66.2)	15.0 (59.0)	48.8
T3	46 (114.8)	29 (84.2)	19 (66.2)	13.7 (56.6)	39
Hot	52 (125.6)	29 (84.2)	19 (66.2)	13.7 (56.6)	39
Extreme	55 (131)	29 (84.2)	19 (66.2)	13.7 (56.6)	39

[a] There is no specification for the outdoor relative humidity as it has no impact on the performance.

[b] Dew-point temperature and relative humidity evaluated at 0.973 atm (14.3 psi).

[c] Per AHRI Standard 210/240.

[d] T3* is a modified T3 condition in which the indoor settings are similar to the AHRI conditions.

Table 4. Performances of Low GWP Alternatives for R-22

	Test Condition	R-22	N-20B	DR-3	ARM-20B	R-444B	Propane (R-290)
COP	B	3.48	3.04	2.88	3.06	3.02	3.85
			-13%	-17%	-12%	-13%	11%
	A	3.07	2.68	2.57	2.71	2.72	3.30
			-13%	-16%	-12%	-11%	7%
	T3*	2.34	2.05	1.99	2.09	2.15	2.49
			-12%	-15%	-11%	-8%	6%
	T3	2.34	2.06	2.01	2.07	2.17	2.49
			-12%	-14%	-11%	-7%	7%
	Hot	1.98	1.77	1.70	1.76	1.85	2.12
			-11%	-14%	-11%	-7%	7%
	Extreme	1.82	1.64	1.55	1.61	1.69	1.96
			-10%	-15%	-11%	-7%	8%
Capacity, kW	B	6.26	5.42	5.52	6.05	5.53	5.93
			-13%	-12%	-3%	-12%	-5%
	A	6.10	5.25	5.40	5.91	5.58	5.62
			-14%	-11%	-3%	-9%	-8%
	T3*	5.41	4.56	4.81	5.28	5.17	4.90
			-16%	-11%	-2%	-4%	-9%
	T3	5.42	4.59	4.83	5.24	5.19	4.91
			-15%	-11%	-3%	-4%	-9%
	Hot	5.00	4.26	4.41	4.84	4.79	4.50
			-15%	-12%	-3%	-4%	-10%
	Extreme	4.76	4.10	4.21	4.62	4.59	4.33
			-14%	-12%	-3%	-4%	-9%

Table 5. Performances of Low GWP Alternatives for R-410A

	Test Condition	R-410A	R-32	DR-55	L41-2 (R-447A)	ARM-71A
COP	B	3.95	3.99	4.03	3.62	3.94
			1%	2%	-8%	0%
	A	3.40	3.55	3.50	3.22	3.38
			4%	3%	-5%	-1%
	T3*	2.47	2.57	2.63	2.48	2.52
			4%	6%	0%	2%
	T3	2.49	2.59	2.52	2.49	2.48
			4%	1%	0%	0%
	Hot	2.07	2.17	2.14	2.13	2.11
			5%	3%	3%	2%
	Extreme	1.87	1.98	1.93	1.96	1.90
			6%	3%	5%	2%
Capacity, kW	B	5.35	5.46	5.15	4.49	4.97
			2%	-4%	-16%	-7%
	A	5.14	5.42	5.01	4.44	4.75
			5%	-2%	-14%	-8%
	T3*	4.39	4.76	4.42	4.01	4.17
			8%	1%	-9%	-5%
	T3	4.41	4.79	4.27	4.03	4.12
			9%	-3%	-9%	-7%
	Hot	3.98	4.43	3.99	3.77	3.83
			11%	0%	-5%	-4%
	Extreme	3.75	4.23	3.76	3.63	3.62
			13%	0%	-3%	-3%

As indicated in Table 4, all R-22 alternative refrigerants have smaller cooling capacities, and only propane provides better COPs than R-22. Table 5 reveals that R-32 leads to larger capacities and COPs than R-410A, and DR-55 lead to similar capacities and COPs as R-410A. Other refrigerant drop-ins of the R-410A alternative refrigerants result in smaller capacities and lower COPs at Conditions of B and A. At high ambient temperatures, i.e. Conditions of T3, T3*, Hot and Extreme, all R-410A alternatives show better COPs, because the R-410A performance degrades drastically when the ambient temperature approaches its critical temperature, i.e. 71.34°C.

This article presents a follow-up study, to reveal physics behind the comparisons in Tables 4 and 5. The experimental data was used to calibrate a physics-based equipment model, i.e. ORNL Heat Pump Design Model, developed by Rice and Shen (1981 and 2014). The calibrated model is able to translate the experimental results to

key parameters, i.e. compressor efficiencies, refrigerant side two-phase heat transfer coefficients, corresponding to each refrigerant.

Thermodynamic properties of Low-GWP alternative refrigerants

The temperature-enthalpy diagram of a refrigerant illustrates two critical properties: its span between the saturated liquid line and saturated vapour line (i.e. latent heat of vaporization) and critical temperature (working range). Volumetric vaporization heat, i.e. latent heat × Vapour Density at similar mid-point temperatures, indicates the evaporating capacity per volumetric flow rate. Refrigerants with smaller volumetric vaporization heat have reduced cooling capacities at a constant mid-point temperature and compressor displacement volume, as with the case with drop-in performance evaluation of replacements.

The evaporation mid-point temperature is impacted by the evaporation heat transfer performance of an alternative refrigerant and the heat exchanger surface area normalized to the evaporating capacity. The heat transfer performance is dictated by two factors, i.e. refrigerant heat transfer coefficient and glide. Glide degrades heat transfer performance in a conventional heat exchanger, which is designed for R-22 or R-410A, due to reduction in average temperature driving potential between the air and the refrigerant. If the heat transfer performance of an alternative refrigerant is worse than the baseline refrigerant, it decreases the suction saturation temperature, and the refrigerant flow rate, due to the decreased UA in the same heat exchanger. Consequently, the cooling capacity of an alternative refrigerant depends on the volumetric vaporization heat and heat transfer performance.

<u>R-22 Alternatives:</u>

For the R-22 alternatives, Figure 1 illustrates the temperature-enthalpy diagram. It can be seen that propane has the widest span between the saturated liquid and vapour lines. Critical temperatures of the refrigerant other than propane are lower than that of R-22.

However, these critical temperatures are all higher than 80°C, and then, impose no limits on the air conditioning application, which tends to have condensing temperature below 70°C. Figure 2 illustrates the volumetric vaporization heat as a function of the average saturation temperature. It indicates that R-22, ARM-20B and R-444B have a similar capacity and other refrigerants have smaller capacities when compared at similar mid-point temperature.

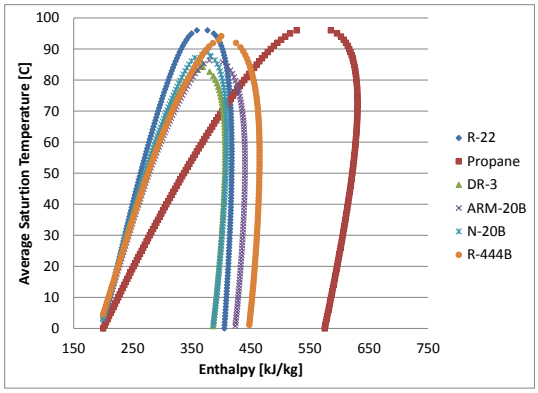

Figure 1. Temperature-Enthalpy Diagram of R-22 Alternatives

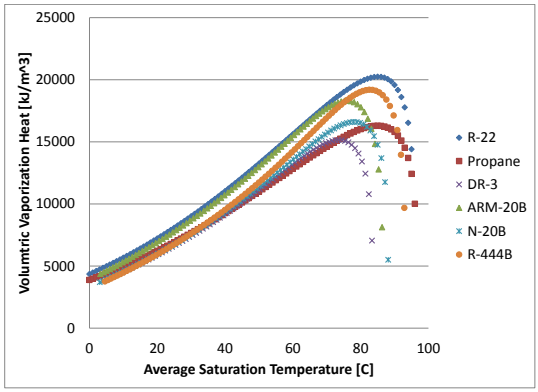

Figure 2. Volumetric Vaporization Heat Diagram of R-22 Alternatives

R-410A Alternatives:

For the R-410A alternatives, Figure 3 illustrates the temperature-enthalpy diagram of each individual refrigerant. The R-410A alternatives all have wider domes and higher critical temperatures than R-410A, indicating they are better refrigerants for high ambient operations. Figure 4 illustrates the volumetric vaporization heat as function of the average saturation temperature. It indicates that R-410A, R-32 and DR-55 have similar volumetric vaporization heat, and R-32 is the largest. Except R-32, the other refrigerants are likely to have smaller cooling capacities if keeping the same heat transfer performance as R-410A.

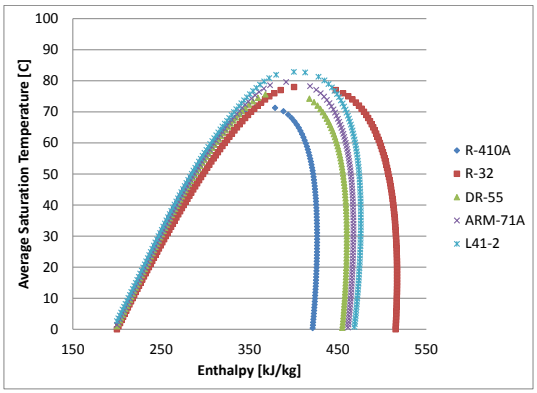

Figure 3. Temperature-Enthalpy Diagram of R-410A Alternatives

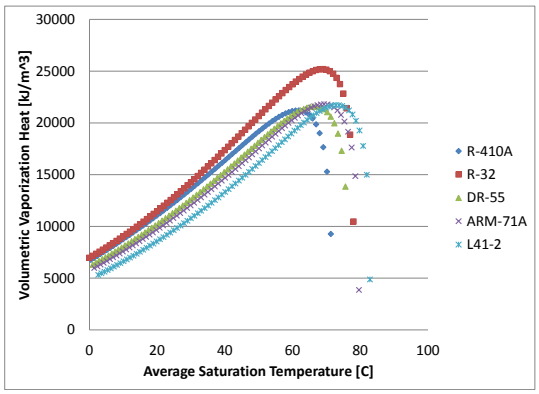

Figure 4. Volumetric Vaporization Heat Diagram of R-410A Alternatives

Besides the thermodynamic properties and heat transfer performance, whether an alternative refrigerant will lead to better cooling capacity and efficiency is also affected by the compressor volumetric efficiency and isentropic efficiency. These will be revealed in the follow sections.

Unit Information

Table 6 describes parameters of the two mini-split air conditioning units. They are single-speed units, having constant indoor and outdoor air flow rates, and compressor speed.

Table 6: Parameters of Mini-Split Air Conditioning Units

Parameters	R-22 Unit	R-410A Unit
Compressor		
Rotational Speed [RPM]	3500	3500
Displacement Volume [cm^3/rev]	29.54	15.2
Outdoor Fan		
Air Flow Rate [m^3/s]	1.203	1.369
Power [W]	180.0	196.0
Indoor Blower		
Air Flow Rate [m^3/s]	0.2832	0.2431
Power [W]	80.7	52.5
Outdoor Heat Exchanger (Condenser)		
Type	Fin-tube coil	Micro-channel
Total Tube Number	52	65
Number of rows	2	1
Number of parallel circuits	(3 condensing +1 subcooling)	(47 cond + 18 in subc)
Fin density (fins/m)	629.9	708.7
Frontal flow area [m^2]	0.587	0.550
Tube diameter [mm]	8.15 (outside diameter)	0.8 (hydraulic diameter)/14 ports
Tube Length [m]	0.89	0.889
Indoor Heat Exchanger (Evaporator)		
Type	Fin-tube coil	Fin-tube coil
Total Tube Number	32	30
Number of rows	2	2
Number of parallel circuits	4	5
Fin density, fins/ft (fins/m)	787.4	787.4
Frontal flow area [m^2]	0.285	0.303
Tube outside diameter [mm]	7.2	6.3
Tube Length [m]	0.813	0.864

During the laboratory investigations, the two mini-split units were instrumented the same way as illustrated in Figure 5. In the figure, the symbol “P” means refrigerant pressure transducers which were placed before the expansion device, and at the evaporator exit. “M” means a refrigerant mass flow meter, which was placed in the liquid line. “W” means Watt transducers, used to measure power consumptions of the compressor, indoor blower and outdoor fan. “T” means temperature probes inserted to refrigerant flow, placed at the compressor suction and discharge, evaporator exit and the liquid line. “Ta” means a temperature sensor to measure the condenser inlet air

temperature. “Ta, RH” means temperature and relative humidity sensors to measure the inlet and outlet states of the indoor air flow.

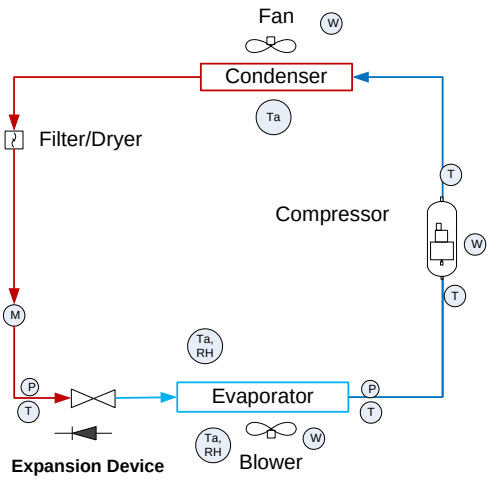

Figure 5. Experimental Instrumentations

Model description

ORNL Heat Pump Design Model (HPDM) is a well-recognized, public-domain HVAC equipment modelling and design tool. It has a web interface to support public use, which has been accessed over 300000 times by US and worldwide engineers. Some features of the HPDM, related to this study, are introduced below:

Compressor model:

In order to model the alternative refrigerants in the same compressor, we used basic efficiencies to model the compressor, i.e. volumetric efficiency shown in Equation 1, and isentropic efficiency shown in Equation 2.

$$m_r = Volume_{displacement} \times Speed_{rotation} \times Density_{suction} \times \eta_{vol} \quad \text{(Equation-1)}$$

$$Power = m_r \times (H_{discharge,s} - H_{suction}) / \eta_{isentropic} \quad \text{(Equation-2)}$$

Where m_r is compressor mass flow rate; $Power$ is compressor power; η_{vol} is compressor volumetric efficiency; $\eta_{isentropic}$ is compressor isentropic efficiency;

$H_{suction}$ is compressor suction enthalpy; $H_{discharge,s}$ is an enthalpy obtained at the compressor discharge pressure and suction entropy.

Heat Exchanger models:

Segment-to-segment fin-&-tube condenser: It uses a segment-to-segment modeling approach, which divides a single tube to numerous mini segments; Each tube segment has individual air side and refrigerant side entering states, and considers possible phase transition; An ε-NTU approach is used for heat transfer calculations within each segment. Air-side fin is simplified as an equivalent annular fin. Both refrigerant and air-side heat transfer and pressure drop are considered; the coil model can simulate arbitrary tube and fin geometries and circuitries, any refrigerant side entering and exit states, misdistribution, and accept two-dimensional air side temperature, humidity and velocity local inputs; the tube circuitry and 2-D boundary conditions are provided by an input file. The flow-pattern-dependent heat transfer correlation published by Thome (2003a, b) is used to calculate the condenser two-phase transfer coefficient. The pressure drop correlation published by Kedzierski (1999) is used to model the two-phase pressure drop.

Segment-to-segment fin-&-tube evaporator: In addition to the functionalities of the segment-to-segment fin-tube condenser, the evaporator model is capable of simulating dehumidification process. The method of Braun et al. (1989) is used to simulate cases of water condensing on an evaporating coil, where the driving potential for heat and mass transfer is the difference between enthalpies of the inlet air and saturated air at the refrigerant temperature. The flow-pattern-dependent heat transfer correlation published by Thome (2002) is used to calculate the evaporator two-phase transfer coefficient. The pressure drop correlation published by Kedzierski (1999) is used to model the two-phase pressure drop. As noted, the segment-to-segment modeling

approach is able to reveal the glide of a zeotropic refrigerant, since the temperature increment is accounted by each individual segment along the refrigerant flow path.

Segment-to-segment micro-channel condenser: The model uses a segment-to-segment modeling approach; each micro-channel port segment has individual air-side and refrigerant-side entering states, and considers possible phase transition; the coil model can simulate arbitrary port shapes (round, triangle, etc.), fin geometries and circuitries (serpentine, slab, etc.). The heat transfer correlation published by Dobson (1998) is used to calculate the condenser two-phase heat transfer coefficient. The Kedzierski (2000) correlation is used to calculate the two-phase pressure drop.

Expansion Devices:

The compressor suction superheat degree and condenser subcooling degree are explicitly specified. As such, the expansion device is not solved here – a simple assumption of constant enthalpy process is assumed.

Fans and Blowers:

Single-speed fan: the air flow rate and power consumption were direct inputs from the laboratory measurements.

Refrigerant Lines:

Heat transfer in a refrigerant line is ignored and the pressure drop is calculated using a turbulent flow model, as a function of the refrigerant mass flux.

Refrigerant Properties:

Interface to REFPROP 9.1: (Lemmon et al., 2010) We programmed interface functions to call REFPROP 9.1 directly; our models accept all the refrigerant types in the REFPROP 9.1 database, and also we can simulate a new refrigerant by making the refrigerant definition file according to the REFPROP 9.1 format.

REFPROP 9.1 can run fairly slow. To speed up the calculation, we have an option to generate property look-up tables, based on REFPROP 9.1; our program uses 1-D and 2-D cubic spline interpolation algorithms to calculate refrigerant properties via reading the look-up tables, this would greatly boost the calculation speed, given the same accuracy;

Model calibration

HPDM has a flexible solver that any variables can be given or solved. That means users can switch between knowns and unknowns in the system solving. For the model calibrations, we input the measured refrigerant mass flow rate, compressor power, the pressure and temperature measurements in Figure 5, as known variables, and then, solve the compressor efficiencies and the two-phase heat transfer coefficients in the condenser and evaporator as unknowns. Two-step solving procedure was applied to decouple the refrigerant side heat transfer and the air side heat transfer. As the HPDM was validated tremendously against R-22 and R-410A units in previous work (Rice 1997, Shen 2005), and thus, its original refrigerant side heat transfer calculations were considered being accurate for the R-22 and R-410A data. For the first step, we reduced the air side heat transfer coefficient for the R-22 and R-410A baseline units using the original refrigerant side heat transfer correlations. As the mini-split units have constant indoor and outdoor air flow rates, the air side heat transfer didn't change when running the other alternative refrigerants. For the second step, we treated the calculated air side heat transfer coefficients as knowns, and calculated the refrigerant side two-phase heat transfer coefficients, specific to each alternative refrigerant. And the phase allocation ratios, i.e. single-phase versus two-phase, are predicted by the HPDM model.

Figure 6 shows calculated volumetric efficiencies as a function of the compressor pressure ratio for the R-22 alternative refrigerants. Figure 7 shows the

isentropic efficiencies. Propane appears to have noticeably better volumetric and isentropic efficiencies than the other refrigerants. One reason is that propane has smaller pressure ratios in the ambient temperature range from 27.8°C to 55°C. The other refrigerants lead to similar efficiencies as R-22.

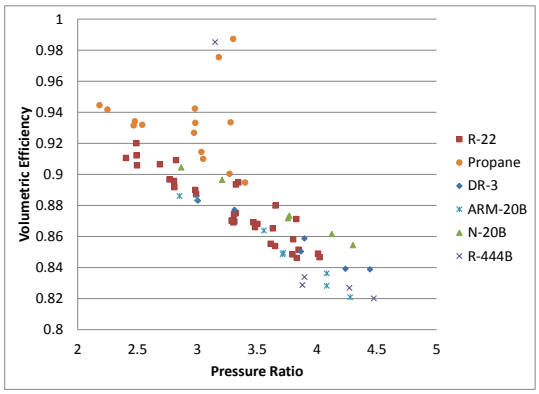

Figure 6. Calculated Volumetric Efficiencies of R-22 Alternative Refrigerants

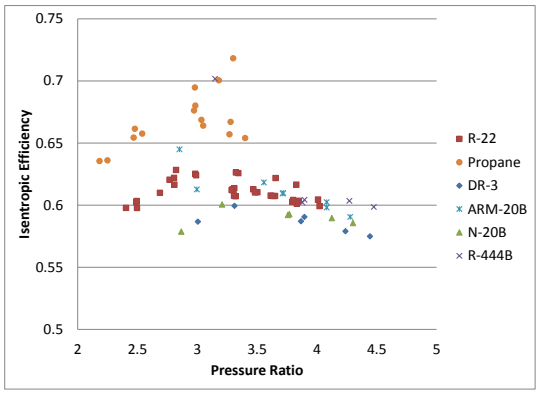

Figure 7. Calculated Isentropic Efficiencies of R-22 Alternative Refrigerants

Figure 8 shows calculated volumetric efficiencies as a function of the compressor pressure ratio for the R-410A alternative refrigerants. Figure 9 shows the isentropic efficiencies. The alternative refrigerants result in no apparent deviations from the R-410A efficiencies. R32 has two outliers, at pressure ratios of 2.43 and 2.92 respectively. These correspond to performance evalution using the originally capillary tube and just optimizing the refrigerant charge at AHRI A and ISO T3 conditions respectively. At these test conditions; the liquid subcooling measured at the mass flow meter inlet was less than 0.6°C (1°F) which suggest that possible flashing in the mass flow meter might resulted in false reading.

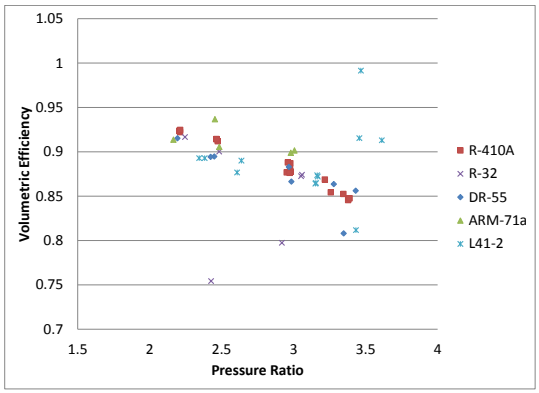

Figure 8. Calculated Volumetric Efficiencies of R-410A Alternative Refrigerants

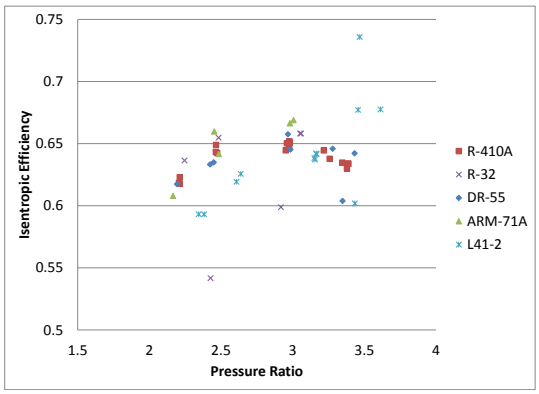

Figure 9. Calculated Isentropic Efficiencies of R-410A Alternative Refrigerants

Figures 10 and 11 show calculated two-phase heat transfer coefficients in the fin-tube condenser and evaporator, of the R-22 alternative refrigerants, versus the ambient temperature respectively. It should be noted that the heat transfer coefficient at one ambient temperature may vary with the indoor wet bulb temperature and the corresponding refrigerant mass flow rate. Furthermore, at the 46°C (115°F) outdoor conditions; there was 2 indoor conditions investigated (T3, and T3*) and there was 3 tests for R-22; using baseline oil; using POE oil; and a re-run using mineral oil at the end. There was also 2 tests for Propane; one with POE oil and one with mineral oil. Figure 10 indicates that R-22 and propane have similar evaporation, two-phase heat transfer coefficients, which are noticeably better than the other alternatives. Figure 11 shows that R-22, propane and ARM-20B have comparable condensation, two-phase heat transfer coefficients, better than the other refrigerants. However, ARM-20B has

temperature glides around 5.3 K (9.5 R) in the condenser, which makes its integrated heat transfer performance worse than the pure refrigerants of R-22 and propane.

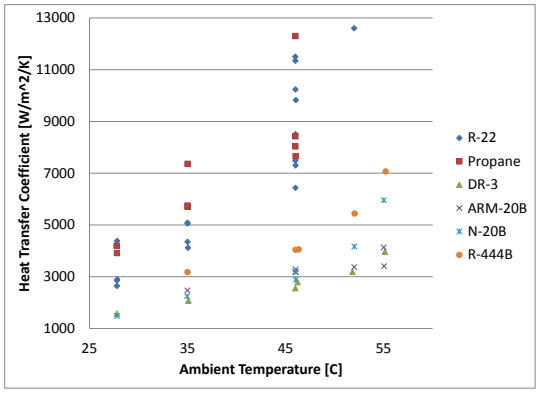

Figure 10. Calculated evaporator two-phase heat transfer coefficients for R-22 alternatives

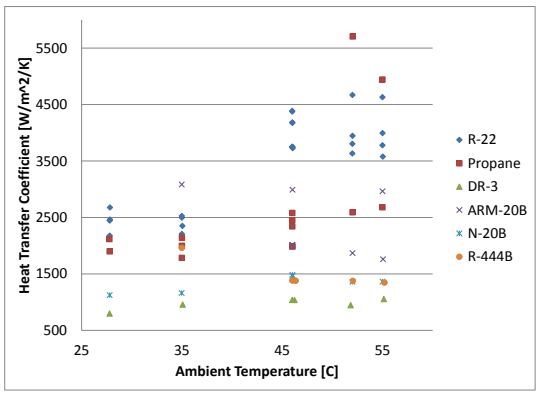

Figure 11. Calculated condenser two-phase heat transfer coefficients for R-22 alternatives

Figures 12 compares the calculated two-phase heat transfer coefficients in the fin-tube evaporator, for the R-410A alternative refrigerants. It can be seen that R-410A has the highest heat transfer coefficients. R-32 is the second highest. ARM-71A and DR-55 have comparable heat transfer coefficients. However, DR-55 should have better integrated heat transfer performance than ARM-71A due to its smaller glide. L41-2 has the worst heat transfer performance, because of its largest glide and smallest heat transfer coefficients.

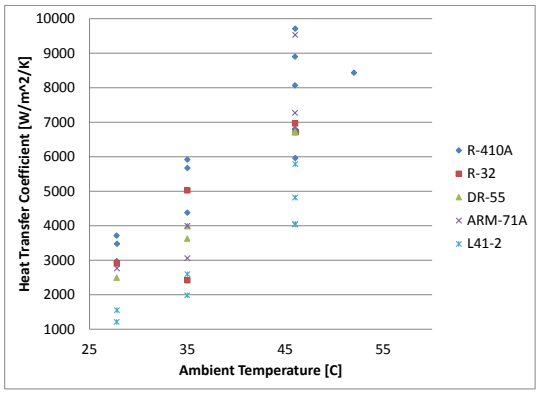

Figure 12. Calculated evaporator two-phase heat transfer coefficients for the R-410A alternatives

Summary

Following the experimental study of Abdelaziz and Shrestha (2016), for low GWP, alternative refrigerants of R-22 and R-410A, we used the HPDM to model the baseline mini-split units and calibrated the models against the experimental data. The calibrated equipment models were used to estimate the compressor efficiencies, and two-phase heat transfer coefficients from this drop-in study. These predicted values provide further insights on the performance of the alternative refrigerants and are useful for other applications beyond mini-split air conditioning units.

By comparing the R-22 alternatives, one can see that R-22 has the highest heat transfer coefficients, no temperature glide and largest volumetric vaporization heat. Consequently, it has larger cooling capacities than the other refrigerants. Propane has similar heat transfer performance as R-22, but smaller vaporization heat. As a result, propane reaches smaller cooling capacities at various ambient temperatures. On the other hand, propane leads to higher COPs than R-22 due to its reduced capacity with the same heat exchangers and increased compressor efficiencies. Except propane, all other R-22 alternatives have lower capacities and efficiencies than R-22 because of their

smaller volumetric vaporization heat, degraded heat transfer coefficients, and temperature glides.

By comparing the R-410A alternatives, one can see R-410A has the best heat transfer performance. R-32 and DR-55 have slightly lower heat transfer performance. R-410A and DR-55 have similar volumetric vaporization heat, smaller than the other alternatives. R-32 has the largest volumetric vaporization heat. Therefore, R-32 leads to the highest cooling capacity and COP at various ambient temperatures. DR-55 has similar capacities and COPs as R-410A. Although ARM-71a and L41-2 have higher volumetric vaporization heat than R-410A, they result in lower capacities and COPs, due to the decreased heat transfer coefficients and larger temperature glides.

References

Abdelaziz, O., and Shrestha S. 2016. Soft-Optimized System Test of Alternative Lower GWP Refrigerants in 1.5-ton Mini-Split Air Conditioning Units. AHRI low-GWP AREP Conference, Jan 2016. http://www.ahrinet.org/App_Content/ahri/files/RESEARCH/AREP_Final_Reports/AHRI_Low_GWP_AREP_Rpt_062.pdf

ASHRAE, 2002, Adiabatic capillary tube selection, Refrigeration Handbook, ch. 45, pp.45.26-45.30, ASHRAE.

Braun. J.E., Klein. S.A, and Mitchell, J.W., 1989, "Effectiveness models for cooling towers and cooling coils", ASHRAE Transactions, 95(2), pp. 164-174.

Dobson M. K. and Chato J. C., 1998 "Condensation in Smooth Horizontal Tubes", Journal. Heat Transfer 120(1), 193-213 (Feb 01, 1998)

Kedzierski, M. A., and Choi J. Y., "A generalized pressure drop correlations for evaporation and condensation of alternative refrigerants in smooth and micro-fin tubes" NISTIR 6333, 1999

Lemmon Eric W., Huber Marcia L. (2010) "NIST Reference Fluid Thermodynamic and Transport Properties Database (REFPROP): Version 9.1", http://www.nist.gov/srd/upload/REFPROP9.PDF

Montreal Protocol, An international agreement reached in 1987 to reduce the production and consumption of chlorofluorocarbons (CFCs) and halon substances.

Ozone Secreteriat, 2016, "The 1987 Montreal Protocol on Substances that Depelete the Ozone Layer", UNEP, http://ozone.unep.org/en/handbook-montreal-protocol-substances-deplete-ozone-layer/27571 accessed April 25th 2016.

Ramanathan and Y. Xu (2010). "The Copenhagen Accord for Limiting Global Warming: Criteria, Constraints, and Available Avenues," Proc. Natl. Acad. Sci. USA 107, 8055–8062.

Rice, C.K., 1981, "Design optimization and the limits of steady-state heating efficiency for conventional single speed air-source heat pumps", Contract No. W-7405-eng-26, ORNL/CON-63, Department of Energy; web link: http://web.ornl.gov/~wlj/hpdm/MarkVII.shtml

Rice, C. K., 1997. "DOE/ORNL Heat Pump Design Model, Overview and Application to R-22 Alternatives",3rd International Conference on Heat Pumps in Cold Climates, Wolfville, Nova Scotia, Canada, Aug. 11-12, 1997; Caneta Research, Inc., Mississauga, Ontario, Canada, November, pp.43-66.

Shen, B. and Rice, C. K., 2014, HVAC System Optimization with a Component Based System Model – New Version of ORNL Heat Pump Design Model, Purdue HVAC/R Optimization short course, International Compressor & refrigeration conferences at Purdue, Lafayette, USA, 2014; web link: http://hpdmflex.ornl.gov/hpdm/wizard/welcome.php

Shen, B, E. A. Groll, and J. E. Braun, 2006. RP-1173 -- Improvement and Validation of Unitary Air Conditioner and Heat Pump Simulation Models at Off-Design Conditions, ASHRAE Research Project Report.

Thome J.R. and Jean Ei Hajal, 2002, "On recent advances in modelling of two-phase flow and heat transfer", 1st Int. Con. on Heat Transfer, Fluid mechanics, and Thermodynamics, Kruger Park, south Africa TJ1, 8-10 April.

Thome J. R., J. El Hajal, and A. Cavallini, 2003a, "Condensation in horizontal tubes, part 1: two-phase flow pattern map", International Journal of Heat and Mass Transfer, 46(18), Pages 3349-3363.

Thome J. R., J. El Hajal and A. Cavallini, 2003b, "Condensation in horizontal tubes, part 2: new heat transfer model based on flow regimes", International Journal of Heat and Mass Transfer, 46(18), Pages 3365-3387.

Xu. Y, D. Zaelke, G.J.M. Velders, and V. Ramanathan (2013). “The Role of HFCs in Mitigating 21st Century Climate Change,” Atmos. Chem. Phys. 13, 6083–6089.

Yana Motta, S. Theoretical and experimental analysis of the flow through adiabatic capillary tubes: zeotropic mixtures and its contamination with oil. Pontificia Universidade Catolica do Rio de Janeiro DSc thesis, Department of Mechanical Engineering, Brazil, 1999.